Behavioral/Systems/Cognitive

Suppressive Surrounds and Contrast Gain in Magnocellular-Pathway Retinal Ganglion Cells of Macaque

Samuel G. Solomon,[1] Barry B. Lee,[2,3] and Hao Sun[2]

[1]Center for Neural Science, New York University, New York, New York 10003, [2]State University of New York, School of Optometry, New York, New York 10036, and [3]Max Planck Institute for Biophysical Chemistry, 37077 Göttingen, Germany

The modulation sensitivity of visual neurons can be influenced by remote stimuli which, when presented alone, cause no change in the ongoing discharge rate of the neuron. We show here that the extraclassical surrounds that underlie these effects are present in magnocellular-pathway (MC) but not in parvocellular-pathway (PC) retinal ganglion cells of the macaque. The response of MC cells to drifting gratings and flashing spots was halved by drifting or contrast-reversing gratings surrounding their receptive fields, but PC cell responses were unaffected. The suppression cannot have arisen from the classical receptive field, or been caused by scattered light, because it could be evoked by annuli that themselves caused little or no response from the cell, and is consistent with the action of a divisive suppressive mechanism. Suppression in MC cells was broadly tuned for spatial and temporal frequency and greater at high contrast. If perceptual phenomena with similar stimulus contexts, such as the "shift effect" and saccadic suppression, have a retinal component, then they reflect the activity of the MC pathway.

Key words: **monkey; contrast gain control; magnocellular; parvocellular; vision; context**

Introduction

The receptive field of spiking visual neurons is classically defined as the region of the visual field in which appropriate stimuli can elicit a change in the firing rate (Hartline, 1938; Barlow, 1953; Kuffler, 1953). It has long been clear, however, that the responses of the classical receptive field (CRF) can often be modified by the simultaneous presentation of stimuli that are incapable of evoking a response themselves. Such an "extraclassical" receptive field (ECRF) is common in neurons throughout the visual pathways of all animals so far investigated, particularly in the visual cortex (Dreher, 1972; Allman et al., 1985; Gilbert and Wiesel, 1990; DeAngelis et al., 1994; Sceniak et al., 1999; Cavanaugh et al., 2002a), but also in the dorsal lateral geniculate nucleus (Levick et al., 1972; Kruger, 1977; Felisiberti and Derrington, 1999, 2001; Jones et al., 2000; Solomon et al., 2002) and retina (Kruger et al., 1975; R. M. Shapley and Victor, 1979; Benardete and Kaplan, 1999). These modulatory signals appear to sum over regions of visual space larger than the CRF, and provide a mechanism through which individual neurons are sensitive not only to the local contrast, but also the spatial context in which this signal is embedded.

Neurons in later stages presumably inherit the functional properties of neurons early in the visual pathway, but we know little about the properties of the ECRF in retinal ganglion cells, particularly in the primate. We establish this here, and find that although the ECRF is a prominent aspect of magnocellular-projecting (MC) ganglion cells, it is mostly absent in ganglion cells that project to the parvocellular (PC) layers of the LGN. In what follows, we concentrate on suppression of the responses of the CRF and distinguish it from the "periphery-effect," an excitatory response first described in cat by McIlwain (1964) and particularly obvious in Y cells. More recently, remote moving patterns have been found to cause an increase or decrease in the discharge rate of cat ganglion cells, depending on the spatial and temporal structure of the stimulus (Passaglia et al., 2001). Periphery-effects are generally weaker in primate retinal ganglion cells and LGN cells (Kruger et al., 1975; Felisberti and Derrington, 2001), which is probably related to the general observation that the spatial nonlinearities exhibited by cat Y cells are rarely found in the primate (Hochstein and Shapley, 1976a; Shapley et al., 1981; Derrington et al., 1984; Blakemore and Vital-Durand, 1986; White et al., 2002). We first show that MC-cell responses to brief probes are generally suppressed by simultaneous changes in surrounding patterns. Using drifting sinusoidal gratings, we then show that suppressive mechanisms surrounding the receptive fields of MC cells are broadly tuned for spatial and temporal frequency and are more effective at high contrasts.

Materials and Methods

General procedures. Experimental procedures have been described in detail previously (Solomon et al., 2005). Briefly, juvenile macaque monkeys (*Macaca fasicularis*; $n = 6$) were initially sedated with intramuscular ketamine (ca. 20 mg/kg^{-1}) and then anesthetized with thiopental (10 mg/kg) for initial surgery. Subsequently, anesthesia was maintained by 1–2% isofluorane in an inspired 70–30% mixture of NO_2:O_2. The electroencephalogram and electrocardiogram were monitored to ensure adequate depth of anesthesia. A venous infusion of 5 mg/kg^{-1} h^{-1} of

Received Feb. 22, 2006; revised July 13, 2006; accepted July 13, 2006.

This work was supported by National Institutes of Health Grant EY 13112 (B.B.L.) and Australian National Health and Medical Research Council Grant 211247 (S.G.S.). We thank J. Kunken for help during experiments and P. R. Martin and C. Tailby for comments on a previous version of this manuscript.

Correspondence should be addressed to Samuel G. Solomon, Department of Physiology/Department of Anatomy and Histology, Building F13, University of Sydney, NSW 2006, Australia. E-mail: samuels@physiol.usyd.edu.au.

DOI:10.1523/JNEUROSCI.0821-06.2006

 0270-6474/06/268715-12$15.00/0

gallamine triethiodide in 6 ml/kg^{-1} h^{-1} of dextrose Ringer solution was used to maintain muscular paralysis. All procedures were approved by the State University of New York Optometry Animal Care and Use Committee, and conform to the Society for Neuroscience Policy on the Use of Animals in Neuroscience Research.

Visual stimuli and cell classification. Visual stimuli were generated using a VSG Series Three video signal generator (Cambridge Research Systems, Cambridge, UK) and presented on a cathode-ray tube monitor (Trinitron; Sony, Tokyo, Japan) at a frame refresh rate of 100 Hz and mean luminance of 40 cd/m^2. The output of the blue gun was set to zero and the monitor was viewed at a distance of 228 cm. All stimuli were viewed through circular or annular apertures with hard edges, with the remainder of the monitor (10 by 7°) held at the mean luminance and chromaticity. Two sets of stimuli were used. In one set, the stimulus was a 45 ms increment or decrement in the luminance of a small circular spot over the receptive field (for on- and off-center cells respectively) presented with or without an annulus surround. The outer edges of the annulus were the edges of the monitor; the inner edge defined a disk of mean luminance, centered on the receptive field, in the center of which the probe was presented. The annulus was filled with a square-wave grating of spatial frequency 0.3 cycles/° and grating contrast was reversed at about the time of probe onset. We measured responses to the probe when the grating contrast reversed at the same time, and before and after the onset of the probe. In pilot experiments, we measured the effect of the remote pattern shift for several probe contrasts. Suppression was always robust in MC cells when the probe contrast was within the dynamic range of the cell, but at low contrasts responses were weaker and difficult to distinguish from the ongoing discharge rate. For the experiments reported here, the probes were 0.1–0.2 Weber contrast in MC cells and 0.5 in PC cells, and in four PC cells we instead used appropriate isoluminant probes. In the other set, the stimuli were horizontal sinusoidal gratings that drifted upward at a rate of 4.3 Hz at a Michelson contrast of 0.75 unless otherwise specified. The gratings could be presented in circular windows (to a maximum diameter of 8°) or in annular windows. For annuli, the outer edge was always a circle 8° in diameter (outside of which the monitor was held at mean luminance); the inner edge defined a disk of the same mean luminance. For circular windows of 8° diameter, and for all annuli, the stimulus was clipped slightly by the edge of the monitor at both the top and bottom. The gratings were homochromatic and modulated in luminance (the red and green guns were modulated in phase) or modulated in chromaticity at photometric isoluminance (the red and green guns were modulated out of phase, providing L- and M-cone contrasts of ~0.15 and 0.34, respectively).

MC cells ($n = 53$) and red–green opponent PC cells ($n = 24$) were distinguished by functional paradigms, including their chromatic response (Smith et al., 1992), contrast sensitivity (Kaplan and Shapley, 1986), and the time course of response to standing contrast (Dreher et al., 1976). Cells with substantial S-cone input were not included in this study. Cells were not usually held long enough to complete all the experiments. Receptive fields were located between 1 and 19° from the fovea (average, 7.4). Our experiments required accurate positioning of the stimulus at the center of the receptive field of a cell. For each cell, the receptive field center was found by adjusting the position of counter-phase modulated bipartite fields oriented horizontally and vertically so that cell response to it was nulled. The position of the receptive field was checked regularly and if it had moved noticeably (a rare occurrence), it was recentered.

Data analysis. Action potentials arising from single units were identified and the time of their occurrence was recorded to an accuracy of 0.1 ms. All our stimuli were periodic and for every set of data we constructed peristimulus time histograms (PSTHs) by averaging many (at least 30) cycles of the stimulus. For responses to brief spots, we averaged normalized PSTHs to determine the latency to peak response for MC and PC cells. Responses for individual cells were based on the average discharge rate in the 72 ms around this latency. For drifting and counter-phase gratings, PSTHs were subjected to Fourier analysis; the first harmonic (F1) amplitude and phase were generally used as a measure of response, but we also extracted the mean (F0) and second harmonic (F2) amplitude for some analyses. We always plot the Fourier amplitudes obtained from the PSTH.

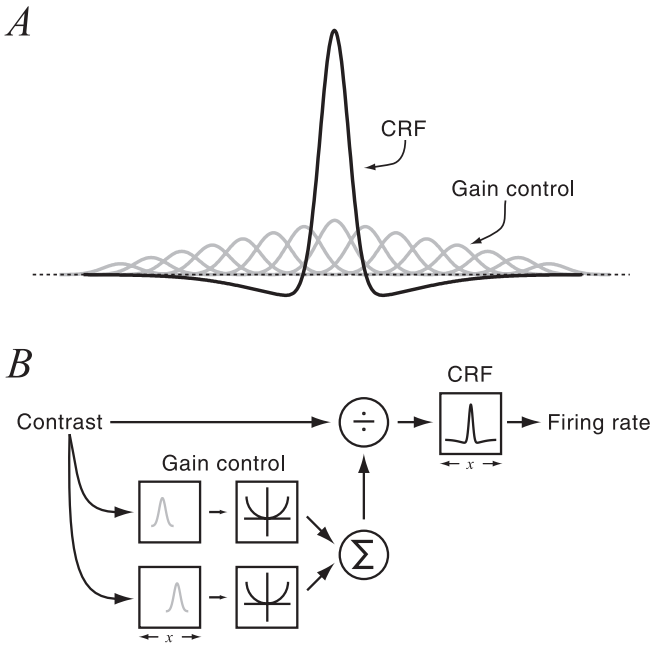

Figure 1. Model of the receptive field of a magnocellular-pathway retinal ganglion cell. ***A***, The spatial distribution of contrast sensitivity for the linear CRF (black line) and ECRF (gray lines). The ECRF is sensitive to the contrast-dependent signals of many subunits distributed over a region of visual space at least as large as the CRF [after Hochstein and Shapley (1976b)]. ***B***, Schematic of the relationship between the CRF and ECRF. Local contrast signals in the CRF are divided by the nonlinearly combined activity of the ECRF subunits.

Models of receptive fields. The classical model of ganglion cell receptive fields is shown by the solid line in Figure 1*A*. The excitatory, center mechanism is concentric with a larger antagonistic surround. The center and surround form the CRF, and this CRF is embedded in an ECRF that regulates its contrast sensitivity. The spatial profile of this ECRF is illustrated by the gray lines in Figure 1*A* (Hochstein and Shapley, 1976b; R. M. Shapley and Victor, 1979). The ECRF accumulates its signal from the output of many small overlapping subunits, which individually have at least as great a spatial resolution as the classical center mechanism. A convenient formulation of the ECRF is to sum the outputs of the subunits after they have been squared (Fig. 1*B*). Combined with the spatial overlap of the subunits, the activity of the ECRF becomes mostly independent of spatial phase (Heeger, 1992).

The spatial sensitivity of the linear receptive field is often modeled by a difference-of-Gaussians function (Rodieck, 1965; Enroth-Cugell and Robson, 1966; Croner and Kaplan, 1995) such that the response of the receptive field to gratings of different spatial frequencies is as follows:

$$R_{(f)} = K_c \pi r_c^2 e^{-(\pi r_c f)^2} - K_s \pi r_s^2 e^{-(\pi r_s f)^2} \quad (1)$$

where K_c and r_c are the gain and size of the center Gaussian and K_s and r_s are equivalent values for the surround; f is the spatial frequency. For most of the experiments described here, it was more convenient to describe the one-dimensional spatial sensitivity of the linear receptive field (CRF) by a single Gaussian, and the spatial sensitivity of the ECRF by a second Gaussian. The activity of each mechanism is determined by the integral under each Gaussian that is covered by the window, such that for the excitatory, classical receptive field, $L_e(d)$ is as follows:

$$L_e(d) = \frac{2}{\sqrt{\pi}} \int_0^d e^{-(x/r_e)^2} dx \quad (2)$$

where r_e is the size of the Gaussian envelope describing the excitatory receptive field and d is the window diameter. A similar equation can be

generated for the ECRF, $L_i(d)$. We believe the ECRF acts as a modulatory signal, incapable of driving the receptive field by itself and, thus, we model its action as divisive and not subtractive. The ECRF acts to suppress the linear receptive field through division, such that the amplitude of the response, G, is as follows:

$$G_{(d)} = \frac{K_e L_e(d)}{1 + K_i L_i(d)} \quad (3)$$

where K_e and K_i are gains for the excitatory CRF and suppressive ECRF (Sceniak et al., 2001; Cavanaugh et al., 2002a). Retinal ganglion cells have spontaneous activity, but their responses are often rectified and can reach maximal firing rates. To accommodate this, we relate the amplitude of the input signal, G, to the measured response, R, with the following:

$$R_{(t)} = R_{\max} \cdot \mathrm{CDF}(G \cdot s_{(t)}) \quad (4)$$

where $s_{(t)}$ is the temporal waveform of the stimulus (in this case a sinusoid), and CDF is the normal cumulative density function (Chichilnisky, 2001). The potential free parameters in this model are the gain K_e and size r_e of the CRF Gaussian, the gain K_i and the size r_i of the ECRF Gaussian, and the three terms that relate generator signal to firing rate: R_{max} and the mean and variance of the CDF. The model was fit simultaneously to the mean rate and amplitude of the fundamental at the temporal frequency of stimulation by minimizing the mean square error of the prediction and data using a Levenberg–Marquet algorithm in the Matlab environment (MathWorks, Natick, MA).

Definition of CRF and ECRF. In the Introduction we defined the CRF of a spiking visual neuron as the region of visual space where presentation of an appropriate stimulus can cause a change in the discharge rate of the neuron. It is impossible to define a priori the set of stimuli that may be able to cause a response from the CRF. Where we investigate the modulation of responses to a central stimulus by an annular one, however, we need some basis for asserting that the impact of the annular stimulus is not caused by stimulation of the CRF. The preceding section makes clear a narrower definition of the CRF: the linear (first-order) component of the neuronal response to modulation of spatiotemporal contrast. In all of our experiments, the contrast of the annular pattern is modulated in time. We have therefore adopted the following rationale: when the annulus alone causes no changes in the linear (first-order) response of the neuron it is not acting through changes in the CRF. This does not preclude the possibility that the neural mechanisms that contribute to the CRF also contribute to the ECRF.

Results

We determined how responses derived from the CRF are modified by the simultaneous presentation of remote stimuli in two quite different experiments. In the first set of experiments, we revisit the impact of large and rapid image translations on the response of ganglion cells to brief pulses of light. In the second set of experiments, we determine the steady state spatial and temporal transfer functions of the ECRF in retinal ganglion cells using drifting sinusoidal gratings.

Suppression of CRF sensitivity by remote pattern shifts

Peripheral stimulation can increase or decrease the discharge rate of ganglion cells; the specifics of this effect are dependent on the type of cell, the spatiotemporal spectrum of the peripheral stimulus, and the ongoing activity from the CRF (Fischer et al., 1975; Barlow et al., 1977; Derrington et al., 1979; Passaglia et al., 2001). Most studies of the periphery-shift effect have used as inducers stimuli far from the center of the CRF (5–40° away); we investigated mechanisms closer to the CRF. The remote pattern was a square-wave grating, counterphase modulated, as sketched in Figure 2*A*. In preliminary experiments on each cell, we measured the discharge rate during reversal of the remote pattern, for inner diameters of the annulus between 1 and 4°. In most MC cells, the discharge rate was modulated at the reversal frequency when the inner diameter of the annulus was 1°. This was not the case when the inner diameter was 2° or greater and we have confined our analysis to the larger diameters.

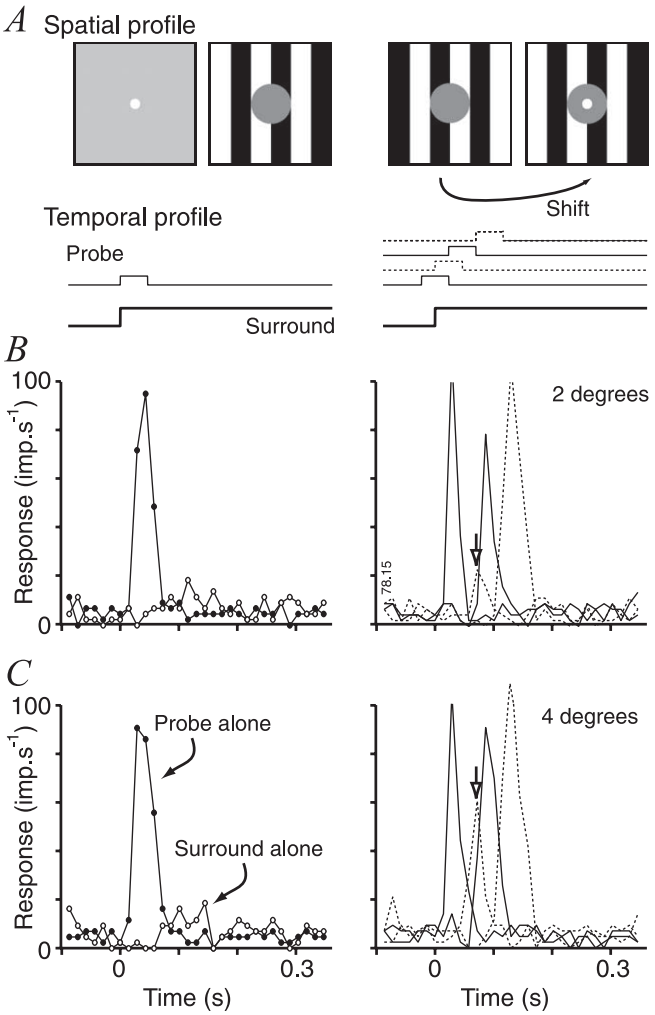

Figure 2. MC-cell response to small brief probes is reduced by the simultaneous modulation of remote patterns. ***A***, Schematic of the spatial and temporal profiles of the stimulus: a probe (diameter 0.5°), centered over the receptive field, was presented for 45 ms; a surrounding square-wave grating (0.3 cycles/°) abruptly reversed contrast, equivalent to shifting the pattern by one half cycle, with no stimulus over the receptive field; or, the probe was presented before, during, or after the shift of the surrounding grating. ***B***, PSTH of a representative off-center MC cell to the probe alone and the surround alone (left panel), or presentation of the two together (right panel). Responses to the probe were usually suppressed by a shift in the surrounding pattern. The inner diameter of the annulus was 2°. In the right panel, responses are aligned to the time at which the surrounding grating changed contrast: the probes that gave rise to these responses occurred 23.1 ms before the shift, at the time of the shift, 23.1 ms after the shift or 69.4 ms after the shift. ***C***, Same as B, but the inner diameter of the annulus was 4°. Probe responses are less affected by the remote shift. The arrows indicate maximal suppression of probe responses, achieved when the surrounding grating reversed contrast at the time the probe was presented.

The left panels of Figure 2, *B* and *C*, shows the response of an off-center MC cell to a small brief luminance decrement (a spot with a diameter of 0.5°), and to reversal of an annular, low-spatial-frequency square-wave grating with an inner diameter of 2 or 4°. The rest of the field was held at the mean luminance (Felisiberti and Derrington, 1999, 2001). Without the surrounding grating, the neuron responded robustly to the probe. For this cell, there was a depression of maintained activity when the an-

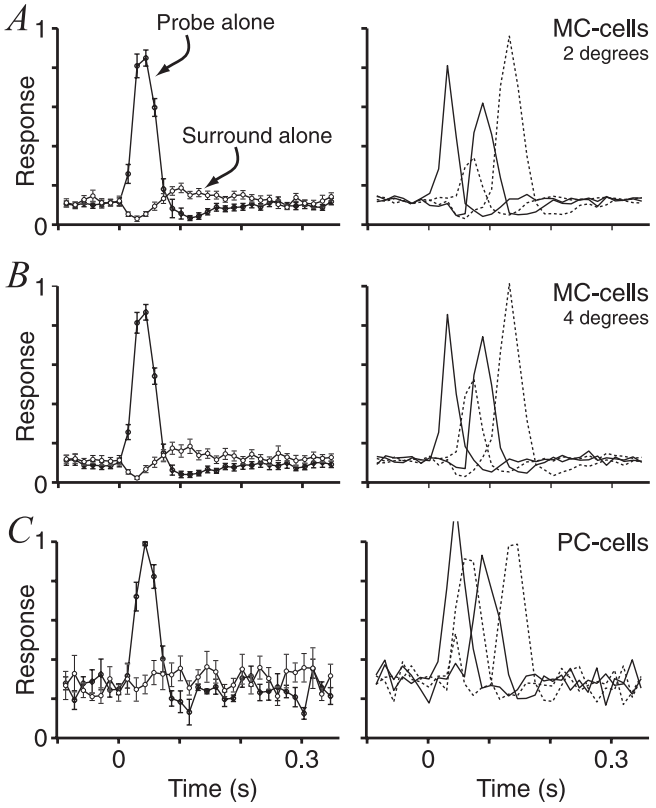

Figure 3. Average responses to probes in the presence and absence of remote pattern shifts. ***A***, ***B***, Average PSTHs of 20 MC cells to the probe alone and the surround alone (left), or presentation of the two together (right). ***A***, The inner diameter of the annulus 2°. ***B***, Inner diameter 4°. ***C***, Average PSTHs of 7 PC cells; same format as ***A***. The inner diameter of the annulus was 1 ($n = 3$) or 2° ($n = 4$). In all cases, responses were normalized before averaging to the maximum firing rate in the probe-alone condition. The time bin in which this maximum was achieved varied across neurons, so the peak of the averaged responses is not necessarily unity. Error bars are 2 SEM. Conventions are as in Figure 2.

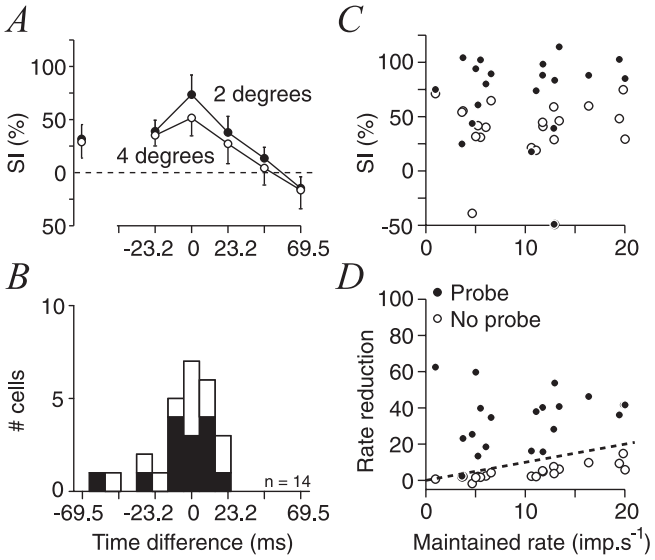

Figure 4. Contrast modulation in surrounding patterns suppresses MC-cell activity most when the CRF is being stimulated at the same time. ***A***, RPS (see Eq. 5) for shifts that occur before, during, and after the onset of the probe. SI shown for annuli with inner diameter 2° (filled symbols) or 4° (open symbols) from the receptive field. Negative time differences indicate that the shift occurred after the onset of the probe. The points on the far left are SI for cell activity in the absence of the probe. Error bars are 2 SEM ($n = 20$). ***B***, Estimates of optimum probe-shift time difference for all MC cells where it could be calculated ($n = 14$; see text). The optimum time is close to zero. ***C***, Suppression of probe responses (filled symbols) is greater than that for maintained activity (open symbols) in individual cells. Annuli were of inner diameter 2°, and the shift occurred at the same time as the onset of the probe. ***D***, Same as ***C***, but showing the actual reduction in spike rate brought about by the shift. The dashed line shows the maximum reduction possible when the probe was absent.

nulus modulated, although the maintained discharge rate of many MC cells could be unaffected by the remote pattern shift; such suppression was difficult to detect if the maintained firing rate was low. The right panels show responses when the probe was presented with different time delays after the reversal of contrast of the annular grating. Depending on the delay, the response of MC cells can be strongly attenuated. Maximum attenuation (arrowed) occurred when the onset of the stimulus and the contrast reversal of the annular grating were simultaneous. Reliable attenuation of probe responses by the peripheral grating was found in all but one of the 20 MC cells studied (12 on-center and 8 off-center) but was weak or absent in PC cells. We investigated relatively few PC cells in this paradigm because no suppression was obvious. Figure 3, *A* and *B*, shows, in the same way as Figure 2, *B* and *C*, the average responses of the 20 MC cells, and Figure 3*C* shows the average responses of the seven PC cells.

To quantify the impact of the remote pattern shift, we determined the change in the probe response (SI_{RPS}) in percentage:

$$SI_{RPS} = 100 \cdot \frac{Resp_{probe} - Resp_{probe+shift}}{Resp_{probe}} \quad (5)$$

where $Resp_{probe+shift}$ and $Resp_{probe}$ are the neuron responses in the presence and absence of the remote pattern respectively. Over all of the MC cells we studied, when presented at the same time as the probe, annuli with an inner diameter of 4° caused an average 49.1% (SD, 38.6) reduction in the response to the probe, but only an average 29.1% (SD, 31.7) reduction in the maintained discharge; maintained rate was, in all cells, less affected by the reversal of the grating. This can be seen Figure 4*C*; it was not just because spontaneous activity was low, as shown in Figure 4*D*. Remote patterns therefore have a greater impact on the probe response of MC cells than on their maintained discharge, whether we considered either the absolute or proportional reduction in discharge rate. The annular stimulus was more effective when the inner diameter approached the CRF; at 2°, probe responses were suppressed by 73.6% (SD, 40.13%) and the maintained discharge by 36.9% (SD, 31.0%). By comparison, PC-cell responses were suppressed by 11.7% (SD, 7.9; $n = 7$) by annuli of inner an diameter of 1 ($n = 3$) or 2° ($n = 4$).

To determine the dependence of suppression on the time delay between the remote pattern shift and the CRF stimulus, the probe was presented before, during, and after the shift. The effectiveness of the remote pattern depended on the time of the shift relative to the probe onset, with the greatest suppression occurring when the remote shift and probe occurred simultaneously (Figs. 2, 3, 4*A*). In most cells, shifts that occurred more than ~50 ms before the probe were incapable of suppressing cell response, and sometimes facilitated it. We estimated the time of the remote shift that generated the greatest suppression, t_{opt}, as the center of mass:

$$t_{opt} = \frac{\sum_{i=1}^{N} SI_i \cdot t_i}{\sum_{i=1}^{N} SI_i} \quad (6)$$

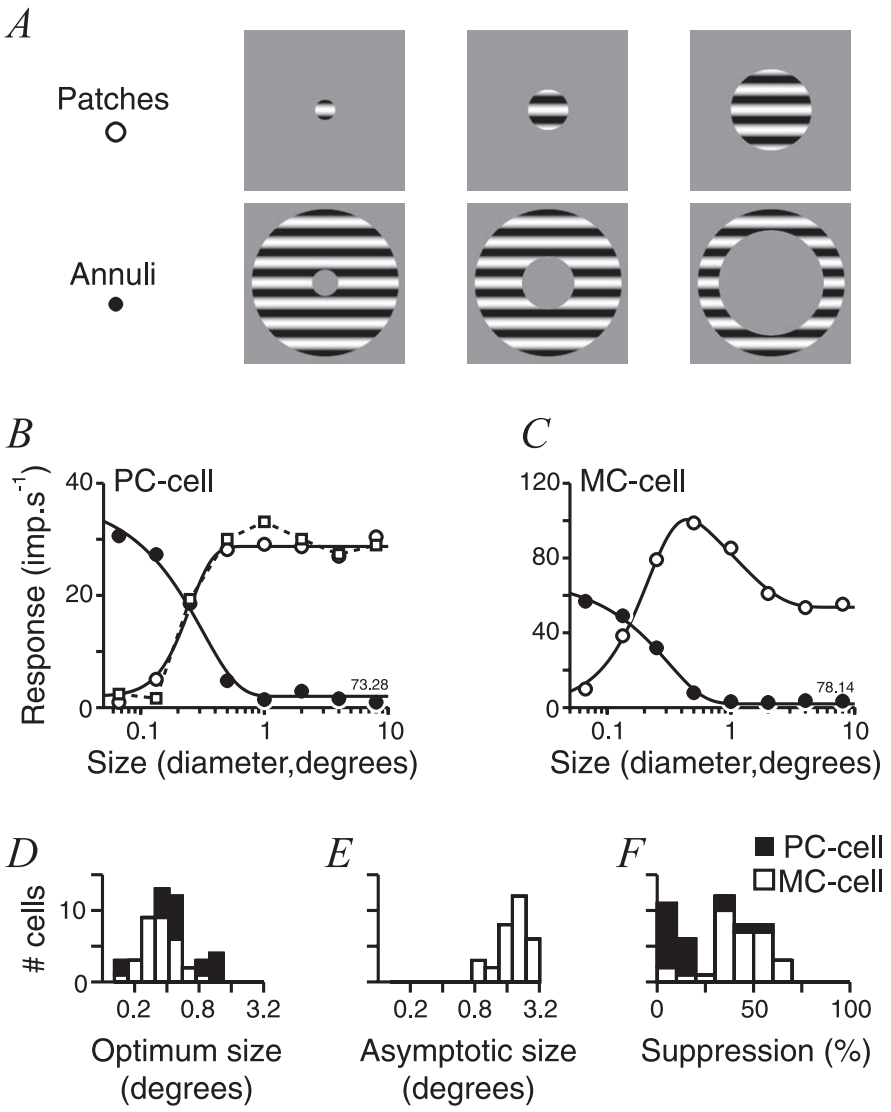

Figure 5. Spatial summation in retinal ganglion cells. ***A***, Schematic illustrations of stimuli used. Horizontal gratings drifted upward at 4.3 Hz; they were visible through circular apertures (patches) or circular annuli. ***B***, Responses of a PC cell to the annuli (filled circles), patches of luminance grating (2 cycle/°; open circles), and patches of chromatic grating (0.1 cycle/°; open squares). Response to the patches monotonically increases. ***C***, Responses of an MC cell to annuli and patches of luminance grating (1 cycle/°). Responses increase until the patch is a diameter of 0.5°, and then decline. Conventions are as in ***B***. ***D***, Distribution of optimal patch diameter for luminance gratings for PC (filled bars) and MC cells (open bars). ***E***, Diameter at which patch response reaches asymptotic values. The distribution of values for MC cells is shown. ***F***, SI (see Eq. 7) for luminance gratings for PC and MC cells. Values in ***D–F*** were determined from fits of Equation 4 to cell responses (smooth lines in ***B***, ***C***).

where N is the number of time differences (t) sampled and SI is the magnitude of suppression at each time difference. Over all MC cells in which suppression was strong enough for us to quantify its effect ($SI_{RPS} > 20\%$), the most suppressive shift was one that followed the probe by 3.5 ms (SD, 39.3; $n = 14$) (Fig. 4*B*). This remained the most effective timing at different annulus sizes. The probe itself lasted 45 ms, and this analysis does not distinguish suppression early and late in the cells response to it. Nevertheless, it is clear that signals from the contrast-reversal of the remote pattern rapidly and transiently suppressed cell sensitivity.

Suppression from remote patterns did not depend on the spatial phase of the annular grating (data not shown). This suggests that the mechanisms giving rise to the suppression are rectified. In a subset of cells, we manipulated the spatial frequency of the annular pattern to try to determine the spatial tuning of the peripheral mechanism. The standard stimulus was a spatial frequency of 0.3 cycles/°; increasing spatial frequency reduced suppression (1 cycle/°, $\mu = 67.4\%$; 4 cycles/°, $\mu = 30.3\%$; $n = 7$) but did not abolish it. The suppressive effect of remote gratings with a sinusoidal spatial profile were almost as effective as those of square-wave gratings. All of this would be consistent with the suppressive mechanism presumably combining nonlinearly the signals of smaller subunits, with spatial frequency acuity as great as that of the MC cell CRF. We did not examine the effect of oscillating the remote pattern at higher temporal frequencies (Passaglia et al., 2001).

Our experiments so far confirm that in MC cells the response of the CRF to visual stimuli can be modulated by a mechanism that acts rapidly and accumulates signals over a large region of visual space. The protocol used resembles psychophysical studies on effects of remote retinal "shifts" on flash thresholds (Breitmeyer and Valberg, 1979; Derrington, 1984). The broad Fourier spectra of the stimuli used so far makes it hard to determine the spatiotemporal sensitivity of the ECRF, or whether stimulation of the ECRF affects functional properties of the CRF other than sensitivity. For the remainder of this study, we use drifting sinusoidal gratings to map the functional properties of the ECRF.

Effect of stimulus size on cell responses to drifting gratings

Figure 5, *B* and *C*, illustrates the responses of a typical PC cell and a typical MC cell to two types of stimuli. Figure 5*B* shows the response (F1) of a PC cell to drifting achromatic gratings viewed through a circular window (open circles), or through an annulus (closed circles). The spatial frequency of the grating was 2 cycles/°, which was slightly higher than the optimal frequency for the cell. As the outer diameter of the window was increased, the grating rapidly encompassed the whole of the CRF and response reached a maximum, after which increasing the diameter of the window further has no effect. The same profile was seen for isoluminant red–green gratings (open squares, spatial frequency 0.1 cycles/°). When the inner diameter of an annulus is made small enough, the grating impinges on the receptive field center and a response is evoked. When the inner diameter of the annulus is large, no response is elicited. This is as predicted for a linear receptive field.

Figure 5*C* shows the response of an MC cell to achromatic gratings, at a spatial frequency of 1 cycle/°. The annulus has the same effect in the MC cell as for the PC cell, evoking responses only when the inner diameter was small. The responses to the windowed grating are qualitatively different. In this case, the responses of the MC cell rapidly increase to a peak, but increasing the diameter of the window further causes the response to decrease. This is incompatible with a linear model and is character-

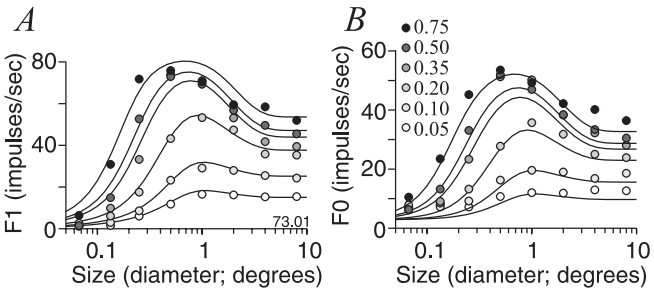

Figure 6. Contrast dependence of spatial summation in an MC cell. ***A***, Amplitude of the modulated response (F1) as a function of size, for six contrast levels. At low contrasts, response increased with size, leveling off at a diameter of 1°. At higher contrasts, the optimum stimulus diameter decreased, and responses were suppressed for large grating patches. ***B***, Average spike rate for the same stimuli. Smooth lines in ***A*** and ***B*** are the predictions of the model described in the text. The stimulus was 1 cycle/°, drifting upward at 4.3 Hz.

istic of suppression by a stimulus incapable of driving the CRF; for example, between 0.5 and 2° from the receptive field, annular gratings evoked no response from the cell but were capable of suppressing the responses evoked from the classical receptive field.

The window diameter for optimal response averaged 0.34° (geometric mean; SD, 0.16; $n = 31$) for MC cells (Fig. 5*D*) and the response then asymptotes at its minimal level at a diameter of 1.82° (SD, 1.22) (Fig. 5*E*). The average inner diameter of the annulus that was capable of evoking a response was intermediate between these two estimates ($\mu = 0.85°$; median, 0.64) and had a wide range (SD, 1.38). We think that this variation is attributable to small errors in centering of the receptive field, elongation of the receptive field along oblique axes, or small eye movements during the experiment. The lower range of these sizes is probably more representative of the underlying receptive fields. Annuli that were unable to generate a modulated response also had little effect on the maintained discharge rate; we first found the largest annulus inner diameter that caused a modulated response, then the maintained discharge rate for the next largest diameter. On average, the maintained discharge with these annuli was slightly less than that when the whole monitor was at the mean luminance, but this was not significant ($\mu = 11.8\%$; SD, 33.4; $p = 0.09$, Student's t test).

To quantify the impact of expanding the window diameter on the magnitude of response, we determined an index similar to that used above (Eq. 5);

$$\mathrm{SI} = 100 \cdot \frac{\mathrm{Resp}_{\mathrm{opt}} - \mathrm{Resp}_{\mathrm{large}}}{\mathrm{Resp}_{\mathrm{opt}}} \quad (7)$$

where $\mathrm{Resp}_{\mathrm{opt}}$ was the response to the optimal window size and $\mathrm{Resp}_{\mathrm{large}}$ was the response to the largest diameter tested (8°). For MC cells, suppression index (SI) was on average 41.3% (SD, 14.4), much greater than it was for PC cells, whether the PC cells were tested with achromatic gratings ($\mu = 14.8\%$; SD, 16.6; $n = 18$) or isoluminant gratings of spatial frequency (0.1 cycles/°; $\mu = 9.3\%$; SD, 14.5, $n = 10$). The majority of PC cells showed no suppression for achromatic or isoluminant gratings; four of 18 cells showed some effect (Fig. 5*F*).

Effect of contrast on suppression from the ECRF

In LGNs and cortical receptive fields, the effectiveness of the ECRF generally increases with contrast. We found this also to be the case for MC cells in the retina. Figure 6*A* plots the response amplitudes (F1) of an MC cell to gratings of different contrasts, drifting upward at 4.3 Hz. It is clear that the reduction in response brought about by increasing window diameter at high contrast is much less evident at low contrast, the midcontrasts showing intermediate amounts of suppression. Along with increasing suppression, the diameter of the optimal grating was larger at low contrasts. Do these changes reflect contrast dependence of spatial summation on the part of the excitatory receptive field and/or the ECRF, or do they reflect interactions between two mechanisms whose spatial summation is stable in the face of increasing contrast? To address this question, we fit the model of Equation 4 to the responses obtained at different contrasts and tried to account for the data with the constraint that the space constants of the excitatory and suppressive Gaussians were the same for all contrast levels; the gain terms were allowed to vary freely. Figure 6*A* shows the best-fitting solution of the model for that cell, and Figure 6*B* shows counterpart plots for the mean discharge rate (F0). As with another eight MC cells studied, the model accounts for almost all of the observed responses, leaving 2.9% variance of the data (Carandini et al., 1997) unaccounted for with 17 parameters. Allowing the space constants of excitatory and suppressive mechanisms to also vary between contrast levels only improved this to 2.2%, at the cost of an additional 10 parameters. We conclude that the change in response shapes with contrast can be well accounted for by the interaction of independent excitatory and suppressive mechanisms whose spatial profile is not changed in contrast.

The suppressive field of these MC cells was about four times the size of the excitatory field; on average, the excitatory space constant was 0.46° (diameter; SD, 0.10) and the suppressive space constant was 1.90° (SD, 0.36). (The receptive fields of these cells were in the parafovea, at an average eccentricity of 11°.) The contrast-dependant changes in the shape of the size-tuning curves are summarized in Figure 7. For each cell, we calculated from the fitted curves the radius at which response was maximal [the grating summation field (GSF)] (Fig. 7*A*). On average, the GSF at low contrast (0.05) was 1.62 that at high contrast (0.75). We also determined the radius at which response reached its asymptote, and this was little affected by contrast (Fig. 7*A*). The decrease in GSF is mainly accounted for by an increase in the relative strength of the ECRF at high contrasts. Figure 7*B* shows the average gain of the excitatory CRF and suppressive ECRF as a function of contrast; in both cases gain is normalized to that obtained at the highest contrast. The gain of the ECRF increases with a slightly steeper slope, and is therefore relatively more effective at high contrasts. This is shown in Figure 7*C*, where we have plotted the strength of the ECRF estimated from our model fits, and for comparison the SI (Eq. 7), obtained from the raw data. From the model, the suppressive effect of the ECRF at one contrast level is obtained with the following equation (Cavanaugh et al., 2002a):

$$\mathrm{SI}_M = 100 \cdot (1 - 1/1 + K_i) \quad (8)$$

where K_i is the gain of the ECRF. In Figure 7*C*, both SI and SI_M increase with contrast. The different contrast–response relationship for the two measures reflects the impact of the spike generation nonlinearity in our model (Eq. 4), particularly by compressing response to strong inputs.

The contrast dependence of spatial summation means that the contrast–response function of MC cells depends on the size of the grating patch used to measure it. This can be seen in Figure 8: in the most effective grating patch for high contrasts (0.25° diameter; stimulus spatial frequency was either 1 or 2 cycles/°, so this

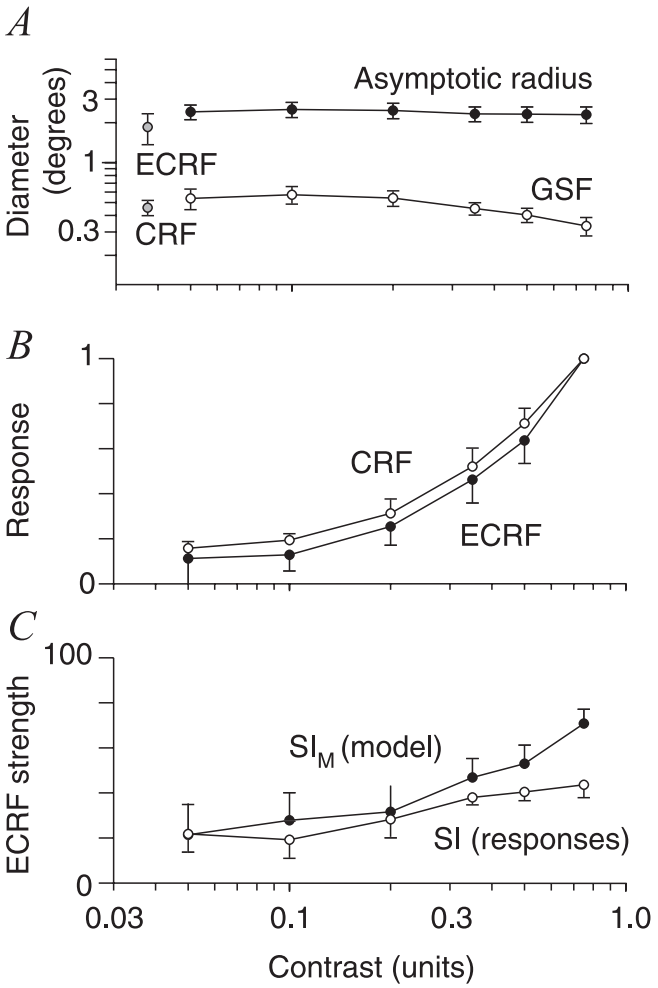

Figure 7. High contrast reduces optimum size in MC cells and increases suppression from surrounding regions. ***A***, MC-cell optimum radius (GSF; open symbols) for patches of drifting grating decreased with contrast. The size at which response reached asymptotic levels changed less (filled circles). ***B***, Response of both CRF (open symbols) and ECRF (filled symbols) increases with contrast, but the slope of the ECRF contrast–response function is steeper. Estimates are based on model fits like that in Figure 4 and were normalized to the response at the highest contrast tested. ***C***, The ECRF is therefore less effective at low contrasts, whether its strength is determined from the model fits (filled symbols; SI_M) or by direct calculation from responses obtained (open symbols; SI). Error bars are 2 SEM and are the average of nine cells.

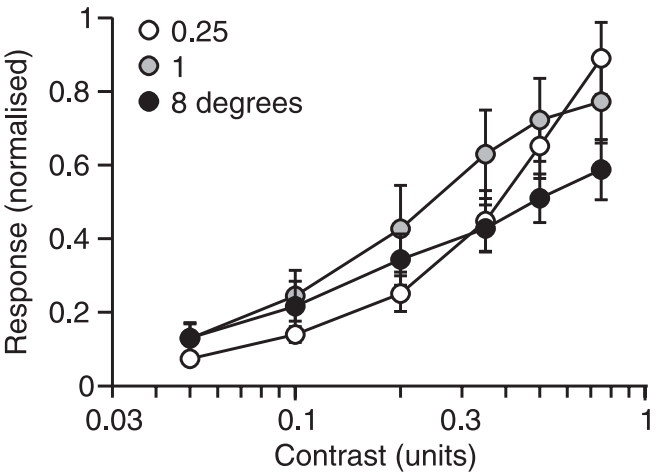

Figure 8. The impact of stimulus size on the contrast response function of MC cells. For optimally sized (diameter 0.25°) patches of drifting grating, MC-cell response increases with contrast. Increasing the stimulus size increases the response at low contrast, but suppresses it at high contrast. Error bars are 2 SEM ($n = 9$). The same cells as in Figure 5 are shown.

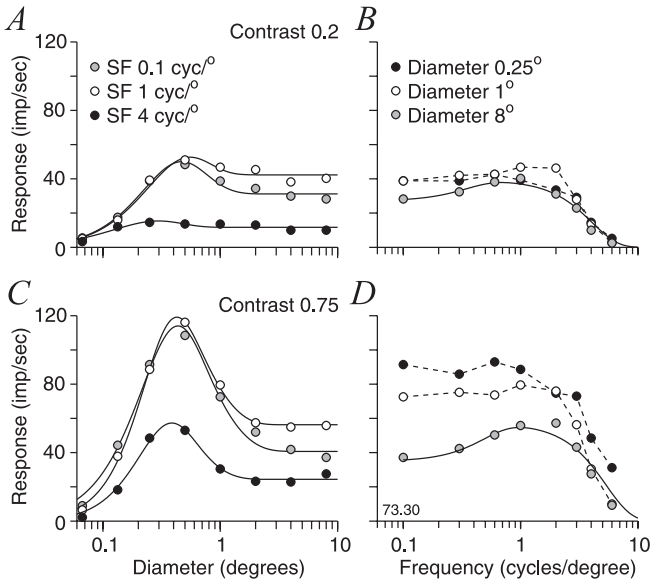

Figure 9. Spatial frequency tuning of CRF and suppressive mechanisms in an MC cell. Responses to a matrix of size and spatial-frequency are shown for drifting gratings of low contrast (***A***, ***B***) or high contrast (***C***, ***D***). Two slices through the matrix are shown: size-tuning is plotted for three of the eight spatial frequencies (***A***, ***C***), or spatial frequency tuning is shown for three of the eight patch diameters (***B***, ***D***). At low contrast, the effect of patch size is strongest at low spatial frequencies. At high contrast, the neuron is tuned for patch size at all spatial frequencies. The smooth lines in ***B*** and ***D*** are fits of a difference-of-Gaussians function to the responses in large patches.

approaches contrast modulation of a spot), responses increase nearly linearly with contrast; enlarging the patch size increases the response at low contrast, but the response at high contrast is reduced. This implies that the ECRF is a major determinant of the shape of the contrast-response function in MC cells.

Contributions of the CRF and ECRF to spatial summation

The response of even a linear receptive field to a drifting grating is a complex interaction of grating size and spatial frequency and the shape of the receptive field, so the CRF itself will be responsible for some of the effects we observe in MC cells (Einevoll and Plesser, 2005). One way to address this question is to determine how size-tuning curves change with spatial frequency: if we know the spatial profile of the CRF, then we should be able to predict its response. We therefore measured response as a function of eight spatial frequencies and eight window sizes at each of two contrast levels (0.20 and 0.75). A representative MC cell is shown in Figure 9, where we have plotted responses at each of three spatial frequencies as a function of window diameter (Fig. 9*A*,*C*) or as a function of spatial frequency for three window sizes (Fig. 9*B*,*D*). Size tuning is more pronounced for higher contrasts (Fig. 9*C*,*D*), as expected. Because spatial summation will reflect both the activity of the CRF and the ECRF, determining the spatial profile of the CRF is not possible directly. We approximated it by making two simplifications. First, we assumed that, at low contrasts, the effect of the ECRF is reduced (compare Fig. 7). Second, we assumed that the minimal suppression at low contrasts is the same at all spatial frequencies; when the stimulus encompasses the whole of the CRF and ECRF, the effect of the ECRF then becomes equivalent to dividing the stimulus contrast by the same amount at all spatial frequencies. Using these assumptions, we took spa-

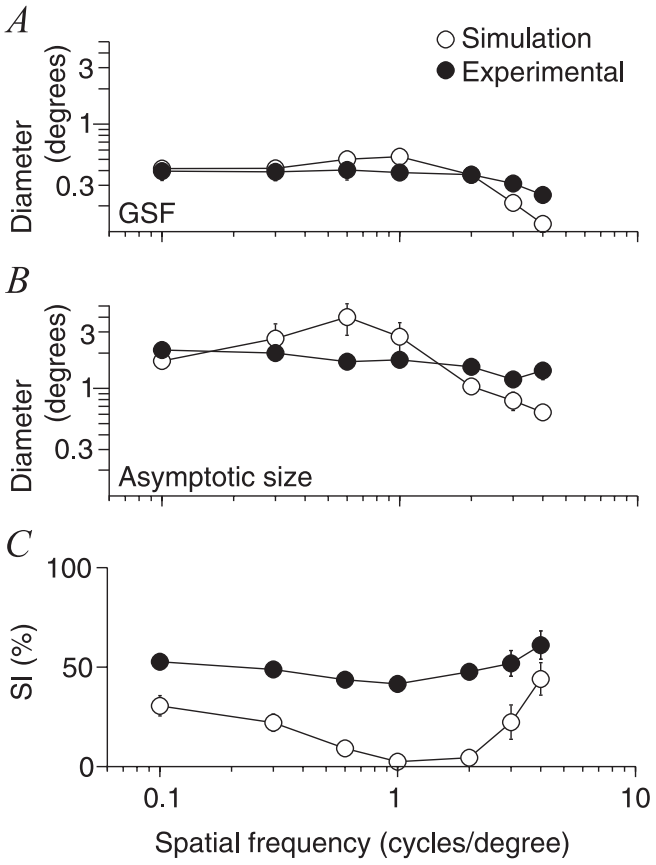

Figure 10. Effect of spatial frequency on size tuning curves. Each panel compares average ($n = 9$) parameters derived from empirical size-tuning curves (contrast 0.75; filled symbols) with those derived from simulations (open symbols; using estimates of receptive field size from a difference-of-Gaussians function fit to low-contrast spatial frequency tuning curves). ***A***, The optimally sized patch of drifting grating is generally predicted by the CRF. ***B***, The patch size where response asymptotes are similar in the prediction and data at low spatial frequencies, but larger in the prediction at mid-range spatial frequencies. This may reflect the lack of size-tuning in the predicted tuning curves at mid-range spatial frequencies, as shown in ***C***. At high spatial frequencies, estimates of GSF and ECRF size from empirical measurements are probably confounded by misalignment of the receptive field and the stimulus. Error bars are 1 SEM.

tial frequency-tuning curves for gratings of contrast 0.20 presented within the largest window, and fit them with the difference-of-Gaussians model of Equation 1 (Fig. 9*B*). For comparison, we also fit the high-contrast versions of these tuning curves (Fig. 9*D*). In agreement with the second assumption, changing contrast had little effect on the shape of the spatial frequency tuning curves: CRF center size was slightly larger at low contrast (average of 113.9%; SD, 14.2; $n = 9$), but the CRF surround size (average diameter, 0.70°) did not change consistently, nor did the relative strengths of the CRF center and surround.

We then extracted the gains and space constants of the CRF center and surround at low contrast and simulated the size-tuning experiments on these linear receptive fields at a variety of spatial frequencies. The simulations confirmed that changing spatial frequency has two main effects on the size-tuning curves of the CRF, both of which are predictable from the Fourier bandwidths of the stimuli and the receptive field. First, the optimal window size decreased at high spatial frequencies. Second, at spatial frequencies both above and below the optimum, response decreased as the window was made larger than optimal. These predictions are compared with the experimental observations (obtained at a contrast of 0.75) in Figure 10: the optimal window size for the simulated CRFs (Fig. 10*A*, open symbols) is in fair agreement with the optimal size of the real neurons, including the decrease in optimal size at high spatial frequencies. This implies that the optimal stimulus size is determined primarily by summation within the CRF. In contrast, the simulation shows no SI for optimal spatial frequencies and does not predict the magnitude of SI at low and high spatial frequencies (Fig. 10*C*). In summary, the size-tuning we find in MC cells cannot be solely attributed to interactions between the stimulus and a linear receptive field. Rather, it is consistent with the action of a suppressive ECRF with broad spatial frequency sensitivity.

The ECRF and frequency-doubled responses

We have so far assumed that the classical receptive field sum signals linearly, but one type of retinal receptive field, "Y-like," shows a second-order nonlinearity in spatial summation because of the presence of receptive field subunits (Enroth-Cugell and Robson, 1966; Hochstein and Shapley, 1976b; Demb et al., 2001). Such nonlinearity is not obvious in the primate retina and LGN (Shapley et al., 1981; Derrington et al., 1984; Blakemore and Vital-Durand, 1986; White et al., 2002), and those cells showing nonlinear spatial summation appear to be the extreme of a continuum rather than a separate cell class. We encountered three MC cells that showed nonlinear spatial summation of this form, showing no null spatial phase for contrast-reversing gratings (Hochstein and Shapley, 1976a). When measured with drifting gratings, size-tuning in these cells was indistinguishable from that in cells that summed linearly. The nonlinearity index (Derrington and Lennie, 1984), a ratio of the second to first harmonic amplitude across spatial phase, was 0.73, 1.16, and 1.25 when tested with counter-phase gratings in a window diameter of 1°; these decreased to 0.16, 0.90, and 0.41, respectively, when the window diameter was 8°. Suppression from the ECRF therefore reduced the second harmonic component of response at least as much as the first harmonic component, suggesting that the ECRF acts before the rectifying nonlinearity.

Effect of ECRF on temporal summation

MC cell responses peak earlier in time and are more transient at high contrast than at low contrast (Benardete et al., 1992; Lee et al., 1994; Chander and Chichilnisky, 2001). In the frequency domain, the temporal modulation transfer function (tMTF) is more bandpass at high contrast, the peak temporal frequency is higher, and response phase advances at midtemporal frequencies. If the ECRF emerges from the same machinery that generates the changes in the tMTF, it should be possible to elicit these effects by enlarging the window rather than increasing the contrast (R. M. Shapley and Victor, 1979). We measured the MC-cell tMTF using drifting gratings (usually 1 cycle/°) at three contrast levels in small (diameter of 1°) or large (8°) windows; the response of a representative MC cell is shown in Figure 11*A*. Making the window large suppressed response to all temporal frequencies at high contrast (0.75) and was not evident for low contrast (0.1) at any frequency. The effect of window size on response phase was less clear (Fig. 11*B*). The inset to Figure 11*B*, which plots response phase against contrast for the responses to 4.3 Hz drifting gratings in small and large windows, shows that the effect of increased contrast is larger than the effect of increased window size. The effect of temporal frequency on suppression from the ECRF is summarized in Figure 11*C*, which shows how expansion of the window suppressed responses at each temporal frequency and contrast. Each point is determined from the average of 10 MC cells tested in this way. Suppression was robust at all temporal

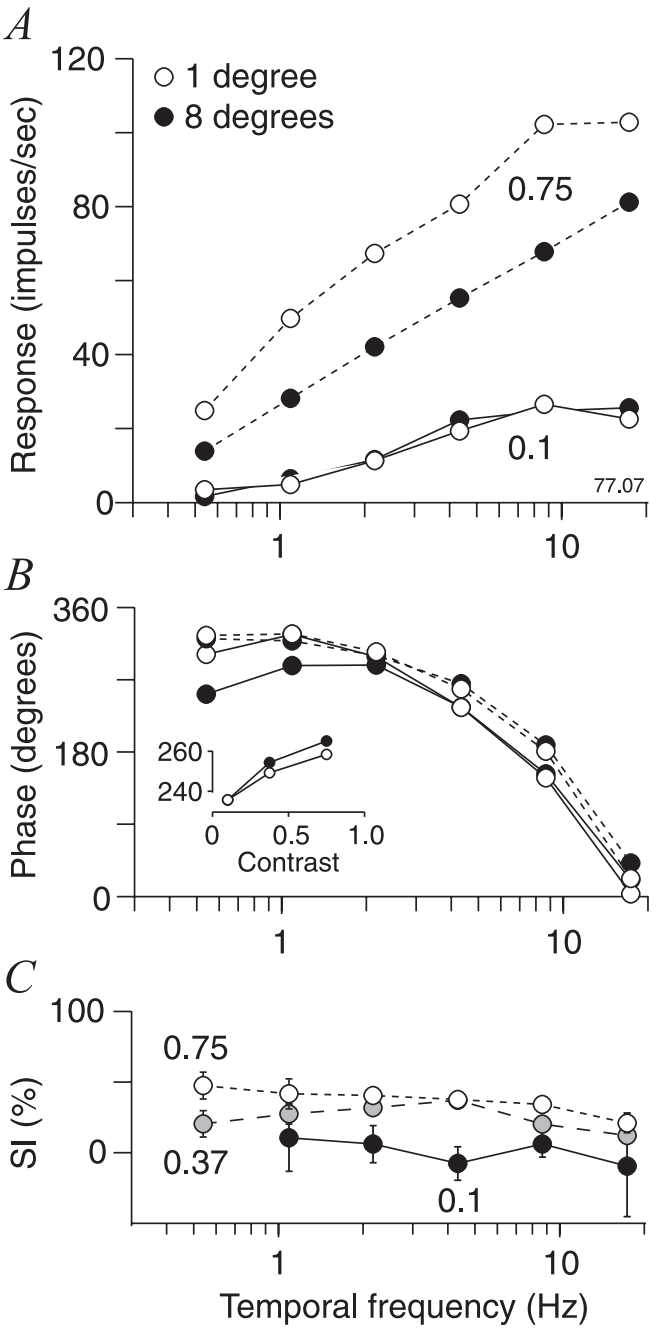

Figure 11. Impact of stimulus size on temporal frequency tuning. ***A***, ***B***, Response amplitude (***A***) and phase (***B***) of one MC cell for drifting gratings presented in windows of 1° (open symbols) and 8° (filled symbols) at each of two contrast levels (dashed lines, 0.1; solid lines, 0.75). Window diameter has no effect on response amplitude or phase at 0.1 contrast; at 0.75 contrast, enlarging the window reduced responses for all temporal frequencies tested, but had little effect on response phase. The inset in ***B*** shows the response phase at 4.3 Hz as a function of contrast for the two window sizes. Contrast has more impact than window size. ***C***, Average reduction in response (SIs) for 10 MC cells at each of the three contrast levels tested. Suppression is greatest at midfrequencies. Error bars are 1 SEM.

frequencies tested. For all cells, response phase advanced with contrast, but was little influenced by the change in window size (data not shown).

Suppression can therefore be accumulated without much change in response phase, but it is possible that in these measurements the effect of ECRF stimulation is swamped by the strong responses evoked from the stimulus over the CRF. One way to remove this confound is to stimulate the ECRF with one contrast while stimulating the CRF with another. We therefore measured responses to drifting gratings presented in a small patch (usually a diameter of 1°), abutting an annulus containing a drifting grating of the same spatial and temporal frequency and phase. [In other experiments not shown, the suppression evoked by the annular grating was found to be independent of its orientation, phase and direction of drift (Solomon et al., 2002).]. The contrasts of the two gratings were varied independently, and from these measurements we constructed contrast response functions for the central patch at each of the annular contrast levels. The responses of a representative MC cell are shown in Figure 12, *A* and *B*. Figure 12*A* plots the response amplitude for the central drifting gratings in the presence of surrounding annuli of three different contrasts. Figure 12*B* shows counterpart plots for the response phase. In this and all nine MC cells tested in this way, response amplitude was reduced by annular gratings, although they could not drive the receptive field. Most (eight of nine) cells showed response phase advance as the contrast of the central patch was increased, and most (six of nine) showed response phase advance when the contrast of the annular grating increased (Fig. 12*C*). The effect is similar in both conditions (average advance 27.9 and 27.8°, respectively). This is equivalent to 18 ms at the temporal frequency used, similar to the contrast-dependant phase advances reported previously in MC cells (Yeh et al., 1995; Levitt et al., 2001). We therefore find that the presence of stimuli that do not directly drive the CRF can nevertheless change response dynamics, suggesting that the ECRF may contribute to the temporal contrast gain control known to exist in MC cells.

Discussion

We have shown that the ECRF contributes substantially to the receptive fields of MC-pathway retinal ganglion cells, and is generally absent from PC-pathway retinal ganglion cells. The suppressive ECRF of MC cells is broadly tuned for spatial and temporal frequency and its strength increases with contrast. The two major retino-geniculostriate pathways therefore carry different representations of spatial contrast: that carried by PC cells is approximately linear, that by MC cells is not. In the following, we address the mechanisms that may underlie these effects and the relationship of our observations to previous studies in subcortical visual pathways, then the potential contribution of the retinal ECRF to cortical processing.

The ECRF and contrast gain control

We show here that the ECRF is strong in MC cells and mostly absent in PC cells of the macaque retina; contrast gain controls are already known to be strong in MC cells and, if present at all, are far weaker in PC cells (Kaplan and Shapley, 1986; Benardete et al., 1992; Lee et al., 1994). In preliminary experiments in macaque LGN, suppressive ECRFs seem strong in MC cells and much weaker in PC cells, if present at all (C. Tailby, N. Dhruv, S. G. Solomon, and P. Lennie, unpublished observations). In the LGN of a New World primate, the marmoset, the ECRF is strongest in MC cells but, although weaker, is still present in PC cells (Solomon et al., 2002; Webb et al., 2002). If the species difference is genuine, this may reflect differences in neural processing in either the retina (marmoset retinal PC cells may have stronger contrast gain controls) or LGN (reflecting differences in local processing or feedback from the visual cortex). X and Y cells in the cat retina and LGN both show contrast gain controls and suppressive ECRFs. The coexistence of these two physiological effects is consistent with the ECRF reflecting the spatial summation of one or

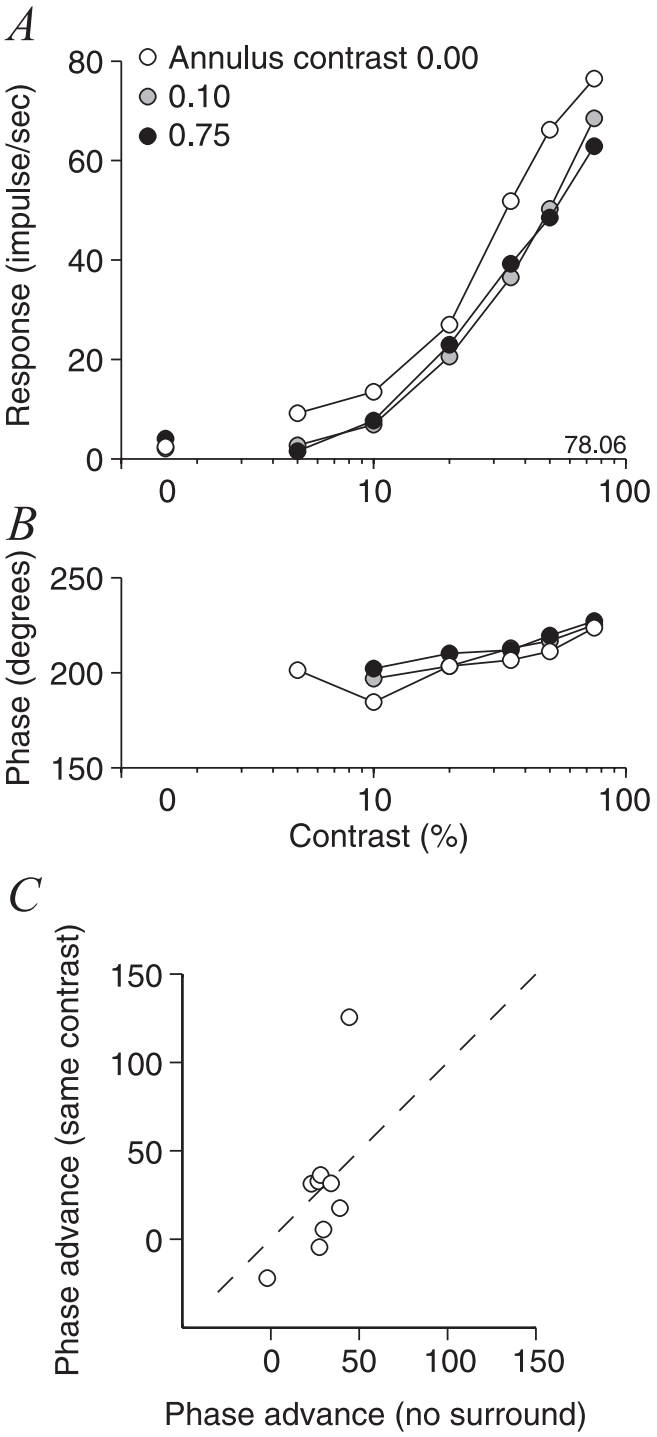

Figure 12. Impact of surrounding patterns on the contrast–response function of MC cells. ***A***, ***B***, Response amplitude (***A***) and phase (***B***) for one MC cell. The stimulus was a drifting grating (1 cycle/°; 4.3 Hz; 1° diameter), which was abutted by an annular grating of the same spatial and temporal frequency at each of three contrast levels (***A***). Response amplitude was reduced at all contrasts, and response phase advanced slightly when the grating over the CRF was at low contrast. ***C***, Comparison of response phase advance calculated for the central stimulus only (the difference between phase at contrast 0.10 and 0.75) and when the central stimulus was contrast 0.10 (the difference between phase at annulus contrasts of 0 and 0.75). Response phase advances for most cells in both conditions are shown.

more contrast gain control mechanisms. The divisive model we used to characterize the ECRF resembles those used for the contrast gain control and a formal relationship between the two has been made previously (Bonin et al., 2005). The simple model is capable of explaining a wide range of observations, including saturation in MC-cell contrast–response curves and size-tuning for drifting gratings.

The link between the ECRF and the contrast-gain control of cat retinal ganglion cells is suggested in the work of Shapley and Victor (Shapley and Victor, 1978; R. Shapley and Victor, 1979; R. M. Shapley and Victor, 1979; Enroth-Cugell and Jakiela, 1980), who further show that in Y cells the contrast gain control occurs before the generation of the frequency-doubled response to contrast reversal. Consistent with this, in the MC cells we encountered with strong second harmonic responses to contrast-reversing gratings, suppression from the ECRF affected the second harmonic amplitude at least as much as the linear response. In cat Y cells, the functional properties of the contrast gain control resemble those of the frequency-doubled response. A reasonable hypothesis is that the contrast gain control arises through feedback to the subunits from their nonlinearly combined activity (R. M. Shapley and Victor, 1979), the subunits themselves the rectifying signals found in some classes of bipolar cell (Demb et al., 2001). Nevertheless, it is not clear that this model is appropriate for primate MC cells and cat X cells, both of which show little frequency doubling (although also weaker contrast-gain control). MC cells do show frequency doubling for chromatic modulation (Lee et al., 1989; Kremers et al., 1994); this is absent if small stimuli are used, the effect increases with stimulus size, and it is strongest at low spatial frequency. However, this nonlinearity appears to be a rectified chromatic signal (Sun and Lee, 2004) and unlikely to be related to the effects described here.

Mechanisms of suppression in retinal ganglion cells

Intracellular recordings from the retina of other animals show that the response of some amacrine cell classes to remote pattern shifts can be very similar to the inhibition that the shift brings about in ganglion cells (Werblin, 1972; Thibos and Werblin, 1978; Roska and Werblin, 2003). These amacrine cells often have large receptive fields and are profoundly nonlinear: they are sensitive to fine gratings and respond at twice the modulation frequency. Inhibition of ganglion cell activity by remote pattern shifts is reduced in the presence of tetrodotoxin, implicating the spiking amacrine cells (Vaney et al., 1988; Demb et al., 1999; Taylor, 1999); these cells are present in the primate retina (Dacey, 1989; Stafford and Dacey, 1997) so their activity may be a source of the suppression seen for remote pattern shifts. It is not clear that size-tuning for drifting gratings can be explained in the same way: substantial suppression could be evoked by stimuli that themselves caused no change in the maintained discharge rate. The biophysical mechanism for such effects remains elusive, although there are several candidates (Carandini and Heeger, 1994; Chance et al., 2002). Inhibition from amacrine cells to the axon terminals of bipolar cells may accommodate the impact of stimulus size on the frequency-doubled response, but inhibition may also be direct on to the dendrites of ganglion cells.

With both remote pattern shifts and drifting gratings we found suppression of visual response. It is still unclear, however, whether common mechanisms underlie the two phenomena. Their spatial frequency tuning was broad, both acted rapidly, and both were insensitive to spatial phase. Although the suppression of maintained discharge was greater for transient changes in remote contrast than with drifting gratings, the discrepancy may be reconciled if the subunits of the ECRF are themselves spatially opponent (with a temporal offset between excitation and inhibition). Center-surround receptive fields are found in bipolar cells

(Dacey et al., 2000) so if the ECRF arises in the inner retina it should inherit this organization.

One argument against a single mechanism underlying all of the effects we describe is that the spatial extent of the ECRF seemed quite different in the two experiments: remote patterns with an inner diameter of 4° were very effective at suppressing probe responses [other studies have shown similar effects for even larger inner diameters (Kruger et al., 1975; Felisberti and Derrington, 2001)], but increasing the diameter of a grating patch from 4 to 8° had little effect on response. If the effectiveness of the ECRF is limited to some maximal value (and thus saturates for strong inputs), expanding the drifting grating may not reveal its full extent. At least in the LGN of the marmoset, ECRFs often show saturating contrast-response and area-response functions (Solomon et al., 2002; Webb et al., 2005a). It is thus possible that the two effects are mediated by a common mechanism, or at least by similar mechanisms with different collection areas. Regardless, functionally they seem to achieve the same effect.

Contribution of retinal ECRF to cortical processing

One aim of this study was to characterize the ECRF in retinal ganglion cells with the types of stimuli used to characterize them in cortical neurons. It is well documented that the ECRF of cortical neurons is often selective for orientation and the direction of movement (Sillito et al., 1995; Levitt and Lund, 1997; Cavanaugh et al., 2002b), and can completely suppress the response of the CRF (Sceniak et al., 2001; Cavanaugh et al., 2002a). These are not the case in the retina or LGN (Solomon et al., 2002; Webb et al., 2002; Bonin et al., 2005) (but see Cudeiro and Sillito, 1996 and references therein), so cortical ECRFs presumably have a cortical component. Nevertheless, it would be surprising if the suppressive mechanisms we observed are not reflected in the activity of cortical cells; simulations suggest they may instead be a major determinant of cortical ECRFs (Cleland et al., 1983; Wielaard and Sajda, 2006). The ECRF of neurons in the monkey striate cortex is broadly tuned for spatial-frequency and temporal-frequency (Webb et al., 2005b), quite unlike the CRF of most cortical neurons; subcortical processing may contribute to this, where the MC pathway is a strong input to the neuron. In the striate cortex of macaque, suppression is strongest in layer IVCα and layer IVB (Sceniak et al., 2001), which receive predominantly MC-cell input: some part of these strong ECRFs may be inherited from MC cells.

Psychophysical thresholds to a brief, flashed probe are increased by simultaneous "shifts" or "jerks" of a peripheral pattern and this has been attributed to the effect to a retinal rather than a central mechanism (Breitmeyer and Valberg, 1979; Derrington, 1984). The time course of the psychophysical effect may be slower and its spatial extent greater than those described here; it is nevertheless plausible that the mechanism characterized here contributes to the psychophysical shift effect, perhaps another example of a psychophysical phenomenon being built from physiological substrates at several loci within the visual pathway. A similar argument may be made for a relation between the effects described and the visual component of saccadic suppression (Mackay, 1970; Burr et al., 1994; Sylvester et al., 2005).

References

Allman J, Miezin F, McGuinness E (1985) Stimulus specific responses from beyond the classical receptive field: neurophysiological mechanisms for local-global comparisons in visual neurons. Annu Rev Neurosci 8:407–430.

Barlow HB (1953) Summation and inhibition in the frog's retina. J Physiol (Lond) 119:69–88.

Barlow HB, Derrington AM, Harris LR, Lennie P (1977) The effects of remote retinal stimulation on the responses of cat retinal ganglion cells. J Physiol (Lond) 269:177–194.

Benardete EA, Kaplan E (1999) The dynamics of primate M retinal ganglion cells. Vis Neurosci 16:355–368.

Benardete EA, Kaplan E, Knight BW (1992) Contrast gain control in the primate retina: P cells are not X-like, some M cells are. Vis Neurosci 8:483–486.

Blakemore C, Vital-Durand F (1986) Organization and post-natal development of the monkey's lateral geniculate nucleus. J Physiol (Lond) 380:453–491.

Bonin V, Mante V, Carandini M (2005) The suppressive field of neurons in lateral geniculate nucleus. J Neurosci 25:10844–10856.

Breitmeyer BG, Valberg A (1979) Local foveal inhibitory effects of global peripheral excitation. Science 203:463–464.

Burr DC, Morrone MC, Ross J (1994) Selective suppression of the magnocellular visual pathway during saccadic eye movements. Nature 371:511–513.

Carandini M, Heeger DJ (1994) Summation and division by neurons in primate visual cortex. Science 264:1333–1336.

Carandini M, Heeger DJ, Movshon JA (1997) Linearity and normalization in simple cells of the macaque primary visual cortex. J Neurosci 17:8621–8644.

Cavanaugh JR, Bair W, Movshon JA (2002a) Nature and interaction of signals from the receptive field center and surround in macaque V1 neurons. J Neurophysiol 88:2530–2546.

Cavanaugh JR, Bair W, Movshon JA (2002b) Selectivity and spatial distribution of signals from the receptive field surround in macaque V1 neurons. J Neurophysiol 88:2547–2556.

Chance FS, Abbott LF, Reyes AD (2002) Gain modulation from background synaptic input. Neuron 35:773–782.

Chander D, Chichilnisky EJ (2001) Adaptation to temporal contrast in primate and salamander retina. J Neurosci 21:9904–9916.

Chichilnisky EJ (2001) A simple white noise analysis of neuronal light responses. Network 12:199–213.

Cleland BG, Lee BB, Vidyasagar TR (1983) Response of neurons in the cat's lateral geniculate nucleus to moving bars of different length. J Neurosci 3:108–116.

Croner LJ, Kaplan E (1995) Receptive fields of P and M ganglion cells across the primate retina. Vision Res 35:7–24.

Cudeiro J, Sillito AM (1996) Spatial frequency tuning of orientation-discontinuity-sensitive corticofugal feedback to the cat lateral geniculate nucleus. J Physiol (Lond) 490:481–492.

Dacey DM (1989) Axon-bearing amacrine cells of the macaque monkey retina. J Comp Neurol 284:275–293.

Dacey DM, Packer OS, Diller L, Brainard D, Peterson B, Lee BB (2000) Center-surround receptive field structure of cone bipolar cells in primate retina. Vision Res 40:1801–1811.

DeAngelis GC, Freeman RD, Ohzawa I (1994) Length and width tuning of neurons in the cat's primary visual cortex. J Neurophysiol 71:347–374.

Demb JB, Haarsma L, Freed MA, Sterling P (1999) Functional circuitry of the retinal ganglion cell's nonlinear receptive field. J Neurosci 19:9756–9767.

Demb JB, Zaghloul K, Haarsma L, Sterling P (2001) Bipolar cells contribute to nonlinear spatial summation in the brisk-transient (Y) ganglion cell in mammalian retina. J Neurosci 21:7447–7454.

Derrington AM (1984) Spatial frequency selectivity of remote pattern masking. Vision Res 24:1965–1968.

Derrington AM, Lennie P (1984) Spatial and temporal contrast sensitivities of neurones in lateral geniculate nucleus of macaque. J Physiol (Lond) 357:219–240.

Derrington AM, Lennie P, Wright MJ (1979) The mechanism of peripherally evoked responses in retinal ganglion cells. J Physiol (Lond) 289:299–310.

Derrington AM, Krauskopf J, Lennie P (1984) Chromatic mechanisms in lateral geniculate nucleus of macaque. J Physiol (Lond) 357:241–265.

Dreher B (1972) Hypercomplex cells in the cat's striate cortex. Invest Ophthalmol Vis Sci 11:355–356.

Dreher B, Fukada Y, Rodieck RW (1976) Identification, classification and anatomical segregation of cells with X-like and Y-like properties in the lateral geniculate nucleus of Old World primates. J Physiol (Lond) 258:433–452.

Einevoll GT, Plesser HE (2005) Response of the difference-of-Gaussians model to circular drifting-grating patches. Vis Neurosci 22:437–446.
Enroth-Cugell C, Robson J (1966) The contrast sensitivity of retinal ganglion cells of the cat. J Physiol (Lond) 187:517–552.
Enroth-Cugell C, Jakiela HG (1980) Suppression of cat retinal ganglion cell responses by moving patterns. J Physiol (Lond) 302:49–72.
Felisberti F, Derrington AM (1999) Long-range interactions modulate the contrast gain in the lateral geniculate nucleus of cats. Vis Neurosci 16:943–956.
Felisberti F, Derrington AM (2001) Long-range interactions in the lateral geniculate nucleus of the New-World monkey, *Callithrix jacchus*. Vis Neurosci 18:209–218.
Fischer B, Kruger J, Droll W (1975) Quantitative aspects of the shift-effect in cat retinal ganglion cells. Brain Res 83:391–403.
Gilbert CD, Wiesel TN (1990) The influence of contextual stimuli on the orientation selectivity of cells in primary visual cortex of the cat. Vision Res 30:1689–1701.
Hartline HK (1938) The response of single optic nerve fibers of the vertebrate eye to illumination of the retina. Am J Physiol 121:400–415.
Heeger DJ (1992) Normalization of cell responses in cat striate cortex. Vis Neurosci 9:181–198.
Hochstein S, Shapley RM (1976a) Quantitative analysis of retinal ganglion cell classifications. J Physiol (Lond) 262:237–264.
Hochstein S, Shapley RM (1976b) Linear and nonlinear spatial subunits in Y cat retinal ganglion cells. J Physiol (Lond) 262:265–284.
Jones HE, Andolina IM, Oakely NM, Murphy PC, Sillito AM (2000) Spatial summation in lateral geniculate nucleus and visual cortex. Exp Brain Res 135:279–284.
Kaplan E, Shapley RM (1986) The primate retina contains two types of ganglion cells, with high and low contrast sensitivity. Proc Natl Acad Sci USA 83:2755–2757.
Kremers J, Yeh T, Lee BB (1994) The response of macaque ganglion cells and human observers to heterochromatically modulated lights: the effect of stimulus size. Vision Res 34:217–221.
Kruger J (1977) The shift-effect in the lateral geniculate body of the rhesus monkey. Exp Brain Res 29:387–392.
Kruger J, Fischer B, Barth R (1975) The shift-effect in retinal ganglion cells of the rhesus monkey. Exp Brain Res 23:443–446.
Kuffler SW (1953) Discharge patterns and functional organization of mammalian retina. J Neurophysiol 16:37–68.
Lee BB, Martin PR, Valberg A (1989) Nonlinear summation of M- and L-cone inputs to phasic retinal ganglion cells of the macaque. J Neurosci 9:1433–1442.
Lee BB, Pokorny J, Smith VC, Kremers J (1994) Responses to pulses and sinusoids in macaque ganglion cells. Vision Res 34:3081–3096.
Levick WR, Cleland BG, Dubin MW (1972) Lateral geniculate neurons of cat: retinal inputs and physiology. Invest Ophthalmol Vis Sci 11:302–311.
Levitt JB, Lund JS (1997) Contrast dependence of contextual effects in primate visual cortex. Nature 387:73–76.
Levitt JB, Schumer RA, Sherman SM, Spear PD, Movshon JA (2001) Visual response properties of neurons in the LGN of normally reared and visually deprived macaque monkeys. J Neurophysiol 85:2111–2129.
Mackay DM (1970) Elevation of visual threshold by displacement of retinal image. Nature 225:90–92.
McIlwain JT (1964) Receptive fields of optic tract axons and lateral geniculate cells: peripheral extent and barbiturate sensitivity. J Neurophysiol 27:1154–1173.
Passaglia CL, Enroth-Cugell C, Troy JB (2001) Effects of remote stimulation on the mean firing rate of cat retinal ganglion cells. J Neurosci 21:5794–5803.
Rodieck RW (1965) Quantitative analysis of cat retinal ganglion cell response to visual stimuli. Vision Res 5:583–601.
Roska B, Werblin F (2003) Rapid global shifts in natural scenes block spiking in specific ganglion cell types. Nat Neurosci 6:600–608.
Sceniak MP, Ringach DL, Hawken MJ, Shapley R (1999) Contrast's effect on spatial summation by macaque V1 neurons. Nat Neurosci 2:733–739.
Sceniak MP, Hawken MJ, Shapley R (2001) Visual spatial characterization of macaque V1 neurons. J Neurophysiol 85:1873–1887.
Shapley R, Victor JD (1979) The contrast gain control of the cat retina. Vision Res 19:431–434.
Shapley R, Kaplan E, Soodak R (1981) Spatial summation and contrast sensitivity of X and Y cells in the lateral geniculate nucleus of the macaque. Nature 292:543–545.
Shapley RM, Victor JD (1978) The effect of contrast on the transfer properties of cat retinal ganglion cells. J Physiol (Lond) 285:275–298.
Shapley RM, Victor JD (1979) Nonlinear spatial summation and the contrast gain control of cat retinal ganglion cells. J Physiol (Lond) 290:141–161.
Sillito AM, Grieve KL, Jones HE, Cudeiro J, Davis J (1995) Visual cortical mechanisms detecting focal orientation discontinuities. Nature 378:492–496.
Smith VC, Lee BB, Pokorny J, Martin PR, Valberg A (1992) Responses of macaque ganglion cells to the relative phase of heterochromatically modulated lights. J Physiol (Lond) 458:191–221.
Solomon SG, White AJ, Martin PR (2002) Extraclassical receptive field properties of parvocellular, magnocellular, and koniocellular cells in the primate lateral geniculate nucleus. J Neurosci 22:338–349.
Solomon SG, Lee BB, White AJ, Ruttiger L, Martin PR (2005) Chromatic organization of ganglion cell receptive fields in the peripheral retina. J Neurosci 25:4527–4539.
Stafford DK, Dacey DM (1997) Physiology of the A1 amacrine: a spiking, axon-bearing interneuron of the macaque monkey retina. Vis Neurosci 14:507–522.
Sun H, Lee BB (2004) The origin of the chromatic response of magnocellular ganglion cells [abstract]. J Vision 4:18a.
Sylvester R, Haynes JD, Rees G (2005) Saccades differentially modulate human LGN and V1 responses in the presence and absence of visual stimulation. Curr Biol 15:37–41.
Taylor WR (1999) TTX attenuates surround inhibition in rabbit retinal ganglion cells. Vis Neurosci 16:285–290.
Thibos LN, Werblin FS (1978) The properties of surround antagonism elicited by spinning windmill patterns in the mudpuppy retina. J Physiol (Lond) 278:101–116.
Vaney DI, Peichl L, Boycott BB (1988) Neurofibrillar long-range amacrine cells in mammalian retinae. Proc R Soc Lond B Biol Sci 235:203–219.
Webb BS, Tinsley CJ, Barraclough NE, Easton A, Parker A, Derrington AM (2002) Feedback from V1 and inhibition from beyond the classical receptive field modulates the responses of neurons in the primate lateral geniculate nucleus. Vis Neurosci 19:583–592.
Webb BS, Tinsley CJ, Vincent CJ, Derrington AM (2005a) Spatial distribution of suppressive signals outside the classical receptive field in lateral geniculate nucleus. J Neurophysiol 94:1789–1797.
Webb BS, Dhruv NT, Solomon SG, Tailby C, Lennie P (2005b) Early and late mechanisms of surround suppression in striate cortex of macaque. J Neurosci 25:11666–11675.
Werblin FS (1972) Lateral interactions at inner plexiform layer of vertebrate retina: antagonistic responses to change. Science 175:1008–1010.
White AJ, Sun H, Swanson WH, Lee BB (2002) An examination of physiological mechanisms underlying the frequency-doubling illusion. Invest Ophthalmol Vis Sci 43:3590–3599.
Wielaard DJ, Sajda P (2006) Extraclassical receptive field phenomena short-range connectivity in V1. Cereb Cortex, in press.
Yeh T, Lee BB, Kremers J (1995) Temporal response of ganglion cells of the macaque retina to cone-specific modulation. J Opt Soc Am A Opt Image Sci Vis 12:456–464.